

● *Original Contribution*

## INVESTIGATION INTO THE MECHANISMS OF TISSUE ATOMIZATION BY HIGH-INTENSITY FOCUSED ULTRASOUND

JULIANNA C. SIMON,\* OLEG A. SAPOZHNIKOV,\*<sup>†</sup> YAK-NAM WANG,\* VERA A. KHOKHLOVA,\*<sup>†</sup>  
LAWRENCE A. CRUM,\* and MICHAEL R. BAILEY\*

\*Center for Industrial and Medical Ultrasound, Applied Physics Laboratory, University of Washington, Seattle, Washington, USA; and <sup>†</sup>Department of Acoustics, Physics Faculty, Moscow State University, Moscow, Russia

(Received 21 July 2014; revised 29 October 2014; in final form 10 December 2014)

**Abstract**—Ultrasonic atomization, or the emission of a fog of droplets, was recently proposed to explain tissue fractionation in boiling histotripsy. However, even though liquid atomization has been studied extensively, the mechanisms underlying tissue atomization remain unclear. In the work described here, high-speed photography and overpressure were used to evaluate the role of bubbles in tissue atomization. As static pressure increased, the degree of fractionation decreased, and the *ex vivo* tissue became thermally denatured. The effect of surface wetness on atomization was also evaluated *in vivo* and in tissue-mimicking gels, where surface wetness was found to enhance atomization by forming surface instabilities that augment cavitation. In addition, experimental results indicated that wetting collagenous tissues, such as the liver capsule, allowed atomization to breach such barriers. These results highlight the importance of bubbles and surface instabilities in atomization and could be used to enhance boiling histotripsy for transition to clinical use. (E-mail: [jcsimon@uw.edu](mailto:jcsimon@uw.edu)) © 2015 World Federation for Ultrasound in Medicine & Biology.

**Key Words:** High-intensity focused ultrasound, Atomization, Histotripsy, Boiling, Cavitation, Capillary wave, Instability.

### INTRODUCTION

Ultrasonic atomization is a process that occurs when an acoustic wave in liquid is directed toward an air interface (a pressure-release interface); the process is not simple when the incident wave is a plane wave, and it becomes even more complex when the incident wave is a narrow, focused beam. Although liquid atomization has been studied extensively since the discovery of atomization in 1927, there remains some doubt as to the exact mechanism (Rozenberg 1973; Simon et al. 2012). The most accepted hypothesis of liquid atomization, called the cavitation-wave hypothesis, states that atomization arises from a combination of cavitation bubble oscillations and capillary wave instabilities (Boguslavskii and Eknadiosyants 1969; Rozenberg 1973). Recently, it was reported that tissues could also be atomized and that such atomization occurs in the form of fractionation and expulsion of tissue from the surface (Simon et al.

2012). Yet questions remain as to the mechanism underlying tissue atomization, particularly the roles of bubbles and tissue properties in the fractionation and atomization of tissue. The goal of the work described in this article was to test experimentally the role of cavitation in the fragmentation and atomization of *ex vivo* tissue by suppressing bubble activity with overpressure. The effects of tissue properties were also investigated, in particular how the wetness of tissue and its surface affect the inception and success of atomization and surface erosion *in vivo* and in tissue-mimicking gels.

Tissue atomization was first explored to explain the mechanism of bulk tissue fractionation in a relatively new high-intensity focused ultrasound (HIFU) approach named boiling histotripsy (Simon et al. 2012). In boiling histotripsy, non-linear propagation effects result in the formation of high-amplitude shocks in the ultrasound pressure waveforms and shock-wave heating causes the formation of a millimeter-diameter boiling bubble at the transducer focus in milliseconds (Canney et al. 2010). Interaction of the incident ultrasound wave with the bubble results in the fractionation of tissue into its submicron components (Khokhlova et al. 2011; Wang et al. 2013).

Address correspondence to: Julianna C. Simon, Applied Physics Lab/CIMU, University of Washington, 1013 NE 40th Street, Seattle, WA 98105, USA. E-mail: [jcsimon@uw.edu](mailto:jcsimon@uw.edu)

With thorough experimentation, it was found that a fountain could form and atomization could occur within a millimeter void that mimicked the HIFU-induced boiling bubble in tissue; that the end result of atomization was erosion of the flat tissue surface adjacent to the air; and that the atomized tissue expelled from the flat tissue surface was partially fractionated, though not to the extent observed in bulk boiling histotripsy (Simon *et al.* 2012). By better understanding the mechanism of tissue atomization, the safety and efficacy of tissue fractionation by boiling histotripsy can be enhanced in its further development and transition into a clinical therapy.

Several observations were made during these preliminary studies, leading to questions regarding the mechanism of tissue atomization. For example, in the initial studies it was observed that the time the *ex vivo* tissue spent submerged in phosphate-buffered saline (PBS) affected the rate of tissue atomization and erosion (Simon *et al.* 2012), leading to the idea that tissue wetness influences atomization. Submersion in PBS is known to cause tissue swelling because of the changes in cellular metabolism and differences in salt and sugar concentrations between the tissue and solution, which affect not only tissue wetness, but also the mechanical stiffness of the tissue (Boutlier 2001; Kaboyashi *et al.* 1991; Southard 2004). In addition, PBS could also influence atomization by forming a thin liquid layer on the tissue surface that could ease the formation of capillary waves or other surface instabilities. Another observation made during preliminary studies was that highly collagenous tissues such as the liver capsule are more difficult to atomize. This relates back to both boiling and cavitation-cloud histotripsy therapies, where it has been noted that highly elastic tissues, such as blood vessels, remained intact while the surrounding tissue was completely fractionated (Khokhlova *et al.* 2014; Vlasisavljevich *et al.* 2014). Investigation into the influence of tissue viscoelasticity and wetness on its atomization could help in determining the tissue types that can be successfully atomized, as well as enhancing our understanding of the fundamentals of the mechanisms of tissue atomization by ultrasound.

In liquids, the cavitation-wave hypothesis most accurately describes what is observed in atomization; however, in tissues there is much debate as to whether atomization can be similarly described. In this article, the hypothesis that bubbles are necessary for tissue atomization was tested. The effect of bubbles was controlled by applying excess static pressure to the tissue samples studied. Overpressure has been used in other ultrasonic applications such as HIFU thermal ablation and shock wave lithotripsy to assess the role of bubbles (Bailey *et al.* 2001; Bronskaya *et al.* 1968; Hill 1971; Khokhlova *et al.* 2006; Sapozhnikov *et al.* 2002). In this work, the role of cavitation in tissue atomization was established using a custom-designed

overpressure chamber and a high-speed camera. In addition, the effect of tissue wetness on atomization was evaluated, considering the relative effects of bulk and surface wetness on the erosion volume in *ex vivo* tissues and tissue-mimicking gels. High-speed photography was also used to analyze atomization *in vivo*, and techniques to breach the collagenous porcine liver capsule were explored. Finally, the hypothesis of tissue fragment recirculation was investigated to explain the histologic differences between bulk boiling histotripsy and atomization. As atomization has been found to explain the mechanism of tissue fractionation in boiling histotripsy, the ultrasound frequency, pulse length and pulse repetition frequency were chosen based on those used in most of the previously reported boiling histotripsy studies (Khokhlova *et al.* 2011, 2014; Wang *et al.* 2013). Although the figures and supplementary videos included in this article illustrate single instances of atomization, they represent what was observed upon repeated experimentation.

## METHODS

### *Effect of overpressure on atomization*

The custom-built overpressure chamber with a 2.127-MHz aluminum-lensed HIFU transducer is illustrated in Figure 1. The transducer consisted of a flat, 40-mm-diameter, piezoceramic source and an aluminum lens with a center thickness of 10.8 mm and a focal length of 40 mm. The static pressure in the chamber was controlled using a compressed air cylinder with a regulator (ProStar 4092, Praxair, Seattle, WA, USA). To create a pressure-release interface at the focal plane with adequate acoustic coupling to the transducer, the lower half of the chamber was filled with water and the tissue sample was placed on a mesh platform with a center cutout and partially submerged in water. In turn, the mesh platform was placed on a hollow acrylic cylinder that fit around the transducer lens. The setup was designed for the distal pressure-release surface of a 1.5-cm-thick piece of tissue to be located in the transducer focal plane; however, with the expectation that the tissue would compress slightly during overpressure, a system was designed to raise and lower the mesh platform. An O-ring was placed in the groove between the aluminum lens of the transducer and the wall of the chamber, underneath the acrylic cylinder. The pipe for the hydraulically controlled water line was placed beneath the O-ring, to allow the hydraulic pressure to raise and lower the tissue, even under increased static pressure conditions. This was essential as once the chamber was sealed, the tissue could not be otherwise manipulated.

Before experimentation, the focal acoustic pressure waveforms generated by the aluminum-lensed transducer were measured in degassed, filtered water with the

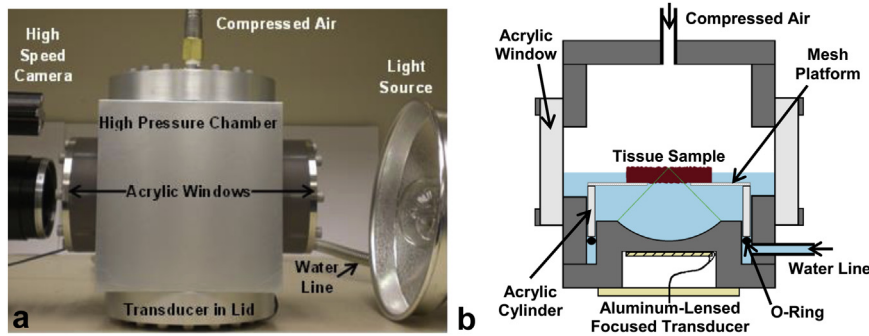


Fig. 1. (a) Photograph of the overpressure experimental arrangement. The overpressure chamber is aluminum-walled with two acrylic windows on opposite sides of the chamber for high-speed photography with backlighting. (b) The internal structure of the overpressure chamber showing the aluminum-lensed transducer built into the lower lid of the chamber, the mesh platform that holds the tissue sample and the hydraulic system including the O-ring and acrylic cylinder that is used to raise and lower the tissue sample once the chamber is sealed.

fiberoptic probe hydrophone (FOPH 2000, RP Acoustics, Leutenbach, Germany). The transducer was driven with a function generator (Model 33250 A, Agilent, Palo Alto, CA, USA) and a linear radiofrequency amplifier (55-dB gain, Model 400 B, ENI, Rochester, NY, USA). The measured acoustic delay to the focus, defined as the location of the maximum peak positive pressure, was 29  $\mu$ s. The intensity at the focus was calculated by integrating the square of the focal pressure waveform distorted by non-linear propagation effects over several cycles and dividing by the sound speed and density as described in Canney et al. (2008). The maximum intensity that could be achieved at the focus in water was 31 kW/cm<sup>2</sup>, with corresponding peak pressures of  $p^+ = 80$  MPa and  $p^- = -19.5$  MPa. The  $-6$ -dB focal dimensions for the peak positive pressures near the maximum intensity level were found to be 0.5 mm transversely and 2.9 mm axially.

*Ex vivo* bovine livers were obtained from a local abattoir (Schenk Packing, Stanwood, WA, USA) and used on the day of harvesting. The liver was cut into sections approximately 5 × 5 cm with thicknesses of 1–1.5 cm, taking care to avoid large blood vessels and remove the capsule from the top surface. All liver exposures consisted of sixty 10-ms pulses repeated at 1 Hz at the *in situ* intensity of 22 kW/cm<sup>2</sup>. (The *in situ* intensity was calculated from measurements in water based on the previously developed derating method for non-linear focused ultrasound fields assuming a liver thickness of 1 cm and an attenuation coefficient of 0.7 dB/cm/MHz [Bessonova et al. 2010; Canney et al. 2010].) Atomization exposures began at atmospheric pressure, after which the static pressure was increased to 1.4 MPa, 2.4 MPa, 3.4 MPa and the maximum pressure that could be safely reached in the chamber, 6.9 MPa. Between each exposure, the chamber was returned to atmospheric pressure and opened to reposition the liver. Each exposure site on the tissue sample was aligned at

pressure with pulse-echo by moving the tissue to obtain the maximum reflected signal amplitude with the timing recorded on a digital oscilloscope (Model 9350 AL, Lecroy, Chestnut Ridge, NY, USA). This indicated the surface of the tissue was at the focus. Exposures were backlit through the two side acrylic windows and recorded. The Photron APX-RS high-speed camera (monochrome, Photron, San Diego, CA, USA) was operated at 10,000 frames per second (fps) with a resolution of 512 × 512 pixels. A Carl Zeiss lens (Makro-Planar, T\*2/100, Thornwood, NY, USA) with a bellows extension was used to provide a resolution on the order of 20  $\mu$ m/pixel. The region of interest was backlit with a continuous, disperse light source (Photogenic PowerLight 2500 DR, Bartlett, IL, USA). From the high-speed videos, emitted particles were sized and the jet velocity was obtained by tracking the particle over several frames as it was emitted from the tissue surface.

At the end of each exposure, the liver surface was photographed and samples were frozen-fixed in Tissue-Tek O.C.T. (optimum cutting temperature) medium for histologic analysis. Alternating 8- $\mu$ m serial sections were stained with hematoxylin and eosin (H&E) to evaluate cellular morphology and nicotinamide dinucleotide diaphorase (NADH-d) to evaluate enzymatic activity as an indicator of thermal injury (Wang et al. 2013). Slides were analyzed on an upright microscope (Nikon Elipse 80 i, Nikon, Melville, NY, USA).

#### Effect of tissue wetness on atomization

**Bulk wetness and atomization.** To evaluate the effect of bulk tissue wetness on atomization, 10 *ex vivo* bovine livers were obtained from the local abattoir and cut into sections as described previously before submersion in one of four solutions of varying salt and sugar concentrations. Solutions included the University of Wisconsin

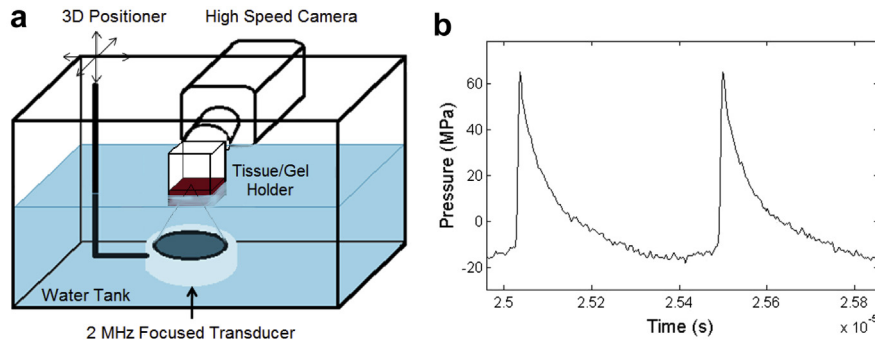


Fig. 2. (a) Diagram of the experimental arrangement for the atomization of *ex vivo* tissues and tissue-mimicking gels. The air-backed piezoceramic focused transducer was submerged in a tank of degassed water, and tissue or gel samples were placed in a custom-designed holder and partially submerged in the water so that their surface, distal from the transducer, was at the transducer focus. Atomization was recorded with a high-speed camera and backlit (not shown). (b) Waveform measured with the fiberoptic probe hydrophone at the focus in water for the maximum output of the spherically focused, piezoceramic transducer. The maximum intensity in water, calculated from the non-linear waveform, was  $22 \text{ kW/cm}^2$  with corresponding maximum measured peak pressures of  $p+ = 65 \text{ MPa}$  and  $p- = -16 \text{ MPa}$ .

ViaSpan (which is commonly used in organ transplantation [Brockbank and Taylor 2006]), phosphate-buffered sucrose (Lam *et al.* 1989), phosphate-buffered raffinose and phosphate-buffered saline (PBS); no solution was also considered. The liver in the no solution group was wrapped in a PBS-wetted towel to prevent the tissue surface from desiccating. Both the phosphate-buffered sucrose and phosphate-buffered raffinose solutions were prepared according to Lam *et al.* (1989) with 120 mmol/L sodium, 60 mmol/L phosphate and 140 mmol/L sucrose or raffinose. The PBS solution was prepared with 0.9% saline. All solutions were degassed in a desiccant chamber at  $-85 \text{ kPa}$  for at least 1 h before the liver samples were submerged.

The experimental arrangement is illustrated in Figure 2a. The liver was placed in a plastic holder with a cutout in the bottom so as not to interfere with the acoustic field. The transducer used for this study was a spherically curved piezoceramic element (PZ 26, Ferroperm Piezoceramics, Kvistgaard, Denmark) with an operational frequency of 2.175 MHz mounted in custom-built polycarbonate housing. The aperture diameter and radius of curvature of the transducer were 45 mm. Focal waveforms of the transducer were measured in filtered and degassed water with the FOPH before experimentation; similar transducers were fully characterized and used in previous boiling histotripsy studies (Canney *et al.* 2008, 2010; Khokhlova *et al.* 2011; Simon *et al.* 2012). The focal waveform measured at the maximum output of the transducer in water is illustrated in Figure 2b.

Atomization exposures were comprised of 10, 30, 60 or 120 ten-millisecond pulses repeated at 1 Hz at the *in situ* intensity in liver of  $16 \text{ kW/cm}^2$  ( $p+ = 53 \text{ MPa}$ ,  $p- = -12.7 \text{ MPa}$ ), which was calculated as described previously. As in the overpressure studies, atomization was backlit and recorded with the Photron high-speed camera.

At the end of the atomization exposures, the eroded tissue was measured with calipers (assuming a precision of 0.5 mm), and the erosion volume was calculated assuming a hemi-ellipsoidal geometry. Tissue wetness was quantified by weighing a small section of the liver sample on the exposure day and after complete desiccation of the same section. Desiccation was achieved by a combination of air-drying on the benchtop and placing the samples in a low-heat oven at  $105^\circ\text{C}$  for at least 48 h until a constant weight was obtained (Little 1964; Sunderman and Williams 1931). The water content was then calculated by taking the difference between the initial and final weights and dividing by the initial weight.

Three samples taken from randomly distributed locations within three livers were submerged in each solution. Within an individual liver sample, each of the four ultrasound pulse numbers was repeated three times separated by at least 6 mm to avoid interactions. For statistical purposes, samples taken from the same liver were considered independent based on structural inhomogeneities and differences in vascularization; the exposure repetition within the same sample were not assumed to be independent. A linear mixed effects model with a random intercept was used to determine whether the solutions affected the erosion volume for the varying number of applied 10-ms pulses. Because of the number of samples,  $p < 0.01$  was considered to indicate significance. (Only a small subset of this study is presented here; further details of the study with an analysis of tissue preservation techniques from acoustic attenuation and sound speed measurements, viscoelastic measurements and histologic analysis are included in the dissertation by Simon [2013]).

*Surface wetness and atomization.* To evaluate the influence of surface wetness on atomization, a tissue-mimicking polyacrylamide gel with 2% bovine serum

albumin was used. Gel was chosen over tissue because of its homogeneity, and the transparency allowed for observations both above and below the viscoelastic surface. The gel was prepared as described by Lafon et al. (2005). Briefly, filtered water was mixed with a 40% (w/v) acrylamide solution (Sigma-Aldrich, St. Louis, MO, USA), a Tris buffer with a pH of 8 and 2% bovine serum albumin. The solution was degassed for at least 1 h in a desiccant chamber at  $-85$  kPa before adding 10% (w/v) ammonium persulfate solution (Sigma-Aldrich), and *N,N,N',N'*-methyleneethylenediamine (Sigma-Aldrich). The solution was poured into seven separate molds with surface dimensions of  $2.5 \times 2.5$  cm at thicknesses of 1–1.5 cm and allowed to solidify.

The experimental arrangement was described previously and is illustrated in Figure 2a. Each of the seven separate gel samples was wetted with one of the seven wetting liquids: water, 70% ethanol, castor oil, glycerol, *n*-propanol, olive oil or 1,3-butanediol. These wetting liquids were chosen as atomization had been attempted previously in the liquids only, with varying levels of success (Simon et al. 2012). Before the gels were wetted, atomization was attempted when the gel surface was dry. Then, a small amount of wetting solution ( $<1$  mL) was added and allowed to spread evenly across the gel surface. With the 2.175-MHz transducer that was described previously, the gel was exposed to sixty 10-ms pulses repeated at 1 Hz at the maximum intensity of  $22$  kW/cm<sup>2</sup> (in water). Exposures were backlit and monitored with the Photron high-speed camera. At the end of the 60 pulses, the gel samples were photographed and measured to record the size of the eroded volume.

#### *In vivo liver atomization*

To validate our extensive *ex vivo* results for clinically related conditions, atomization was studied *in vivo* using a porcine animal model. These studies were approved by the University of Washington Institutional Animal Care and Use Committee. For the studies, the abdomen was opened to expose the liver. A water-filled cone with a Tegaderm membrane and ultrasound gel were used to couple the same 2.175-MHz focused transducer that was described previously to the underside of the liver surface. As the distance from the water-filled cone to the transducer was 1.5 cm, liver sections approximately 1.5 cm thick were selected using pulse-echo and caliper measurements. Because of the breathing motion of the pig, the transducer and the liver were held in place and the position was visually maintained.

*In vivo* atomization exposures were conducted in at least two pigs in locations where the liver capsule was excised (for comparison to bulk *ex vivo* atomization studies) and intact. As preliminary *ex vivo* results indicated that the intact liver capsule was difficult to atomize,

the *in vivo* intact liver capsule exposures were conducted both when the liver capsule was dry and when the capsule was wetted with saline or a surfactant. These wetting liquids were chosen to test the influence of surface tension on the atomization and erosion of the liver capsule. The surfactant was Dawn dish soap mixed in water at a 20 mL soap to 80 mL water ratio with a reported surface tension of 24.5 mN/m (Albaugh et al. 2008), which is approximately one-third the surface tension of water. This corresponds to a calculated capillary wavelength of  $5.1$   $\mu$ m in the surfactant (as compared with  $7.3$   $\mu$ m in water) because the wavelength is proportional to the surface tension raised to the one-third power (Rozenberg 1973). By conducting these studies *in vivo*, disruption of the liver capsule could be identified through bleeding, circumventing the need to visually or histologically find any small fissures in the liver capsule.

The *in vivo* exposures were recorded with the Photron high-speed camera with back and side lighting by the Photogenic light source in addition to top lighting by the lights in the surgical suite. At the end of the exposures, photographs were taken of the liver surface, and samples were removed and fixed in 10% neutral buffered formalin. Samples were embedded in paraffin and 5- $\mu$ m-thick sections were stained with H&E for histologic analysis.

#### *Atomization and recirculation*

Previous histologic results have revealed that atomized tissue fragments expelled from a flat tissue surface are not fractionated to the same extent as was observed in bulk boiling histotripsy (Simon et al. 2012). One possible explanation for this difference could be the recirculation of the tissue fragments within the vapor void formed in bulk boiling histotripsy. Indeed, if the tissue fragments are exposed to HIFU repeatedly, because of the space constraints of the void they will become smaller and smaller after each repeated exposure. To test whether recirculation of the atomized particles caused complete fractionation of the tissue cells, an approximately 3-mm cube of *ex vivo* bovine liver was placed in the bulb of a 1-mL polyethylene pipet. The pipet bulb was partially submerged in water for coupling to the same 2.175-MHz transducer operated with 10-ms pulses at 1 Hz, as described previously. A clamp was placed slightly above the tissue sample to minimize sample motion from the acoustic radiation force while maintaining the tissue–air interface. When the fractionated tissue occluded the tissue–air interface, the remnants of the bulk tissue sample were removed, and the remaining liquefied tissue was further circulated. On removal from the pipet, the recirculated and liquefied tissue was smeared onto a microscope slide and stained with H&E for histologic analysis.

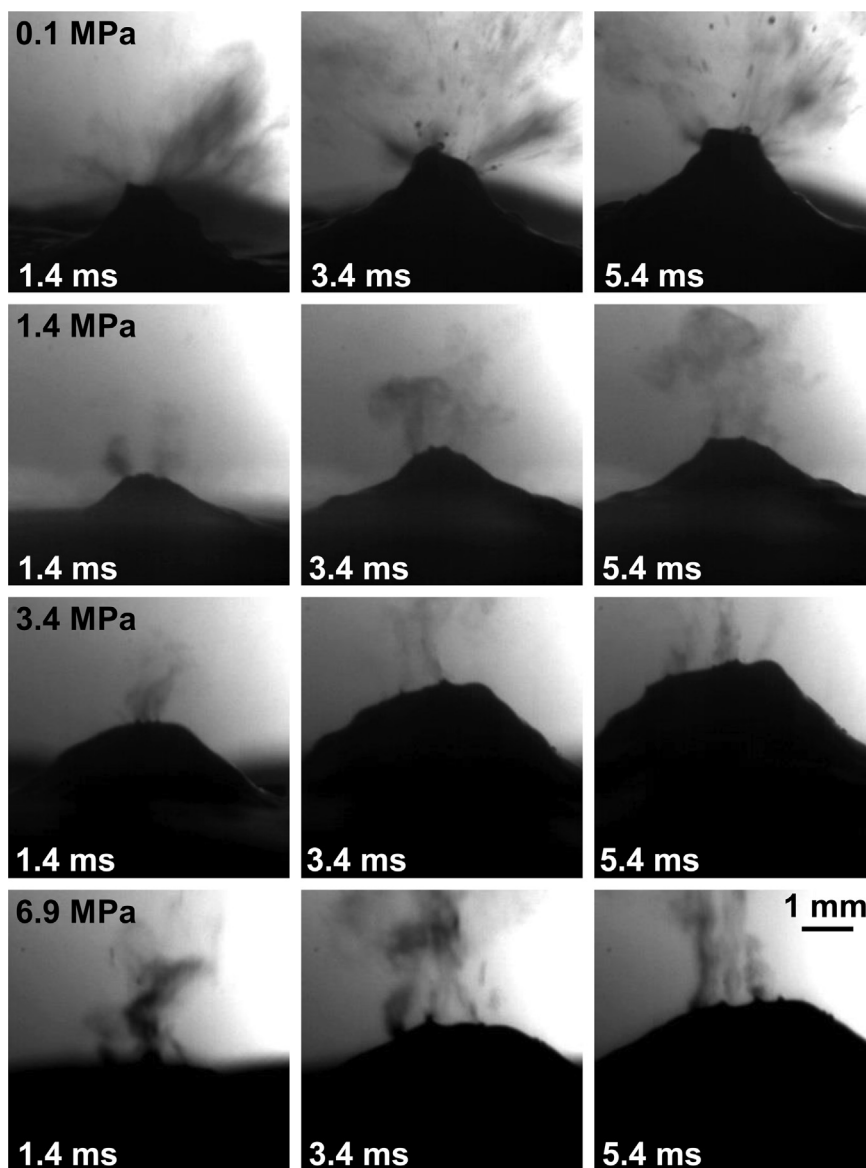


Fig. 3. Select frames from the high-speed videos of overpressure atomization. In the first row, atomization proceeds at atmospheric pressure (0.1 MPa), and 20- to 180- $\mu\text{m}$  droplets are released at 5–7 m/s. When the pressure is increased to 1.4 MPa, droplets are uniformly small (on the order of 20  $\mu\text{m}$  or 1 pixel in diameter) and released at 2–3 m/s. When the pressure is further increased to 3.4 or 6.9 MPa, droplets are still very uniform in diameter (on the order of 20  $\mu\text{m}$  or 1 pixel) and released at the same 2–3 m/s velocity. As the pressure increases, the curvature of the tissue mound becomes shallower with no significant change in mound height. This figure is shown in video format on-line in [Supplementary Video 1](http://dx.doi.org/10.1016/j.ultrasmedbio.2014.12.022) (see the online version at <http://dx.doi.org/10.1016/j.ultrasmedbio.2014.12.022>).

## RESULTS

### *Effect of overpressure on atomization*

As illustrated in [Figure 3](#), at atmospheric pressure and the *in situ* intensity of 22  $\text{kW}/\text{cm}^2$  ( $p^+ = 67.4$  MPa,  $p^- = -16.4$  MPa), atomization of bovine liver with the aluminum-lensed transducer proceeds similarly to what was observed previously ([Simon et al. 2012](#)); droplets are released from a mound in bovine liver at velocities of approximately 5–7 m/s, ranging in diameter

from less than 1 pixel (20  $\mu\text{m}$ ) up to 180  $\mu\text{m}$ . However, when the static pressure is increased even to 1.4 MPa, atomization of bovine liver looks qualitatively different; the emitted droplets are uniformly small (less than 1 pixel [20  $\mu\text{m}$ ] in diameter) and the mound in bovine liver has a more shallow curvature. The uniformly small droplets and decrease in the bovine liver mound curvature continue as the static pressure increases to 2.4, 3.4 and 6.9 MPa, though at 3.4 and 6.9 MPa, an occasional larger

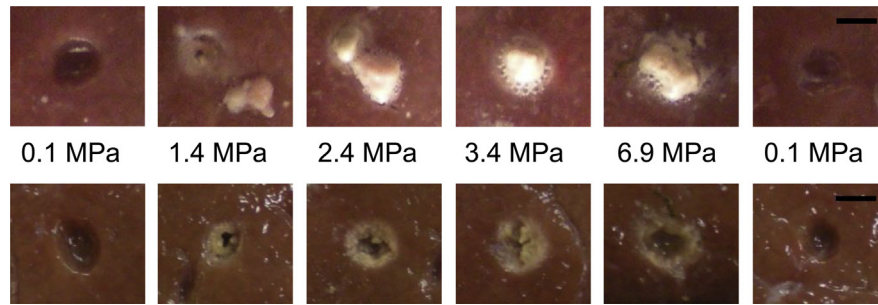


Fig. 4. Upper: Photographs of the liver surface immediately after atomization at different overpressure levels. At atmospheric pressure, a cavity is observed in the tissue surface. The thermally denatured mound of tissue at 1.4 MPa was disturbed during the study; however, the other overpressure levels show the thermally denatured mound that forms after the atomization exposure. Lower: Photographs of the liver surface after blotting to remove excess liquids and the thermally denatured mounds of tissue. As before, a cavity is observed at atmospheric pressure with no evidence of thermal denaturation of the surrounding tissues. When the static pressure is increased, a cavity is still observed (after the mound is removed), surrounded by a thermally denatured tissue border. The final column in the figure illustrates that the cavity in the liver surface when the liver sample was returned to atmospheric pressure did not significantly differ from that of the original atmospheric pressure exposure. Bar = 3 mm.

droplet approaching  $130\ \mu\text{m}$  in diameter is released. Although it is difficult to get an accurate velocity measurement for the fine droplets emitted during overpressure, the estimated velocity is 2–3 m/s for all overpressure levels from 1.4 to 6.9 MPa. When the pressure is again reduced to atmosphere, atomization appears similar to what was observed before the pressure was increased. The mound height does not appear to be correlated with the static pressure level and varies between 2.5 and 3 mm for all levels of overpressure.

At the end of sixty 10-ms pulses repeated at 1 Hz, the tissue surface was photographed both in the chamber (Fig. 4, upper) and after surface blotting (Fig. 4, lower). As expected from initial atomization studies (Simon et al. 2012), a cavity is observed at atmospheric pressure, but when the pressure is increased, a mound of thermally denatured liver is observed at the exposure site. When the liver surface is blotted, this mound of tissue becomes detached, and a cavity is visible in the tissue surface surrounded by a thermal border; no thermal border is evident on gross examination of the cavity from the exposures at atmospheric pressure.

In Figure 5 are histology images of samples at atmospheric pressure (0.1 MPa), 2.4 MPa, and 6.9 MPa. At atmospheric pressure, the histology reveals that the cavity in the tissue surface is approximately 2 mm in diameter and in depth. The NADH-d stain reveals some sections of lighter staining in the cellular debris within the cavity and in some of the cells at the edge of the cavity, indicating reduced enzymatic activity or slight thermal damage to the tissue. At 2.4 MPa, a cavity approximately 1.7 mm in diameter is observed that reaches 3.2 mm below the tissue surface, with enzymatically inactive, or thermally denatured, cells and debris extending from the cavity to the tissue surface and beyond. Upon magnification

of the tissue in the mound above the tissue surface, thermal damage with little to no cellular structure is observed, suggesting that the tissue was partially or completely fractionated before thermal denaturation. However, the tissue in the focal path beneath the tissue surface appears granular, which suggests the tissue was thermally denatured before fractionation. At 6.9 MPa, the degree of tissue fractionation is reduced. Tissue below the surface is thermally denatured but not fractionated; however, the mound above the surface exhibits thermal injury with some granularity, suggesting that the tissue was at least partially denatured before fractionation. At 6.9 MPa, there is no cavity beneath the liver surface, and the tissue has a somewhat triangular or hemi-ellipsoidal pattern of thermal injury that is different than what was observed at lower overpressure levels.

#### *Effect of tissue wetness on atomization*

**Bulk wetness and atomization.** On analysis of the high-speed videos of atomization after submersion of *ex vivo* bovine liver samples in one of the four solutions or in the PBS-wetted towel, there were no obvious differences in the inception of atomization, emitted particle diameters or jet velocities. Statistical analysis of the erosion volume also revealed no difference between the solutions ( $p = 0.48$ ), though the analysis did indicate differences in the erosion volume for the varying number (10, 30, 60, 120) of 10-ms pulses repeated at 1 Hz ( $p = 0.001$ ). Figure 6 is a plot of the percent water content versus the eroded tissue volume for the exposures consisting of sixty 10-ms pulses repeated at 1 Hz. The plot indicates there is no correlation between water content and eroded tissue volume for the tested range of tissue wetness between 55% and 87%.

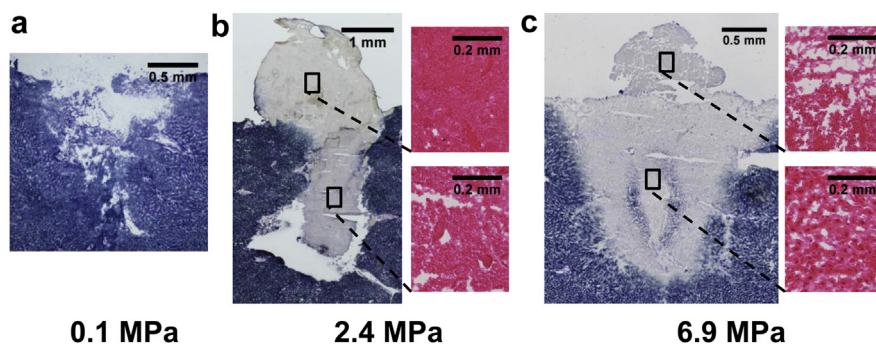


Fig. 5. Nicotinamide dinucleotide diaphorase (NADH-d)- and hematoxylin and eosin (H&E)-stained sections taken from liver treated with sixty 10-ms pulses repeated at 1 Hz in the overpressure chamber. (a) Representative NADH-d-stained sample of the cavity in tissue after atomization at atmospheric pressure. There is a slight lightening of the stain at the tissue borders, indicating some thermal injury as evidenced by the reduced enzymatic activity. (b) NADH-d-stained sample after atomization at 2.4 MPa, with two magnified images taken from an H&E-stained serial section. The NADH-d stain reveals a cavity beneath the tissue surface, with thermally denatured tissue spanning from the cavity to the tissue surface and beyond. On magnification of the tissue in the mound (upper H&E stain), little to no cellular structure is present in the thermally injured tissue; however, on magnification of tissue below the surface (lower H&E stain), the thermally injured tissue is more granular in appearance, indicating partial tissue denaturation before incomplete fractionation. (c) Large NADH-d-stained sample after atomization at 6.9 MPa with two magnified H&E-stained regions. The NADH-d stain reveals a large, thermally denatured tissue region and mound. Note the two areas of blue/purple shading within the thermally denatured region are likely due to staining artifact (Wang *et al.* 2013); the tissue is still thermally denatured. On magnification of the thermally denatured tissue below the tissue surface (lower), the tissue is thermally denatured but not fractionated; however, on magnification of the tissue in the mound (upper H&E), partial tissue fractionation after the thermal denaturation is visible.

*Surface wetness and atomization.* Atomization and fountain formation occurred when the tissue-mimicking polyacrylamide gel surface was wetted with any of the seven liquids (water, 1,3-butanediol, *n*-propanol, castor oil, glycerol, 70% ethanol and olive oil), though not when the gel surface was dry. In Figure 7 are selected frames from the high-speed videos of the dry, water-wetted, 70% ethanol-wetted and glycerol-wetted gel surfaces. These results are summarized in Table 1. In the first row in Figure 7 are selected frames from the video of the dry gel surface where subsurface cavitation and mound formation but no atomiza-

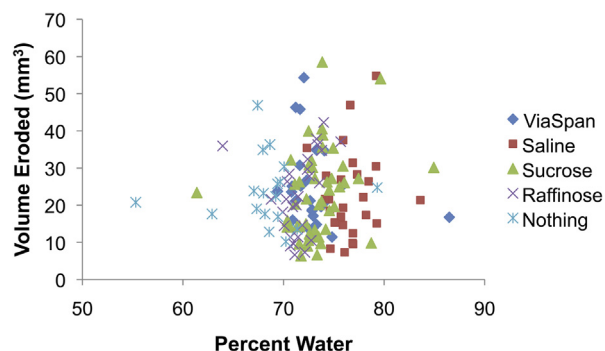


Fig. 6. Plot of tissue wetness versus erosion volume for the exposures of sixty 10-ms pulses repeated at 1 Hz. Although there are several outliers on both axes, there is no correlation between the percent water content and the volume of eroded tissue ( $p = 0.48$ ).

tion is observed. On examination of the gel surface after sixty 10-ms pulses, a mound rather than a cavity is observed in the gel surface because atomization does not occur when the gel surface is dry. Conversely, the frames from the water-wetted gel reveal significant atomization, with jet velocities ranging up to 17 m/s and a relatively homogeneous particle size distribution with diameters on the order of 1 pixel (20  $\mu\text{m}$ ). Subsurface cavitation is present within and below the surface mound. The end result of water-wetted gel atomization is a cavity in the gel. When the gel is alcohol-wetted with 70% ethanol or *n*-propanol (not shown), initial jetting is followed by the formation of a mound that enhances atomization. Jet velocities generally range from 6 to 8 m/s, though some of the initial jets reach 13 m/s, and droplets are one to several pixels in diameter (20–60  $\mu\text{m}$ ). Surprisingly, atomization of the glycerol-wetted gel is more similar to the atomization of the alcohols than to that of castor oil, perhaps because of the hydrolysis of the castor oil by the water-based polyacrylamide gel. With glycerol, a fine mist is ejected before the mound forms and enhances atomization. The diameters of the droplets are very small, with most of them on the order of several pixels ( $\sim 60 \mu\text{m}$ ) in diameter; a few droplets reach 300  $\mu\text{m}$  in diameter. Jet velocities are 4–6 m/s, though a few jets reach 10 m/s. In the videos for all wetting liquids and for the dry surface, cavitation activity is observed beneath the surface. The end result of atomization with any of the wetted gels is a cavity

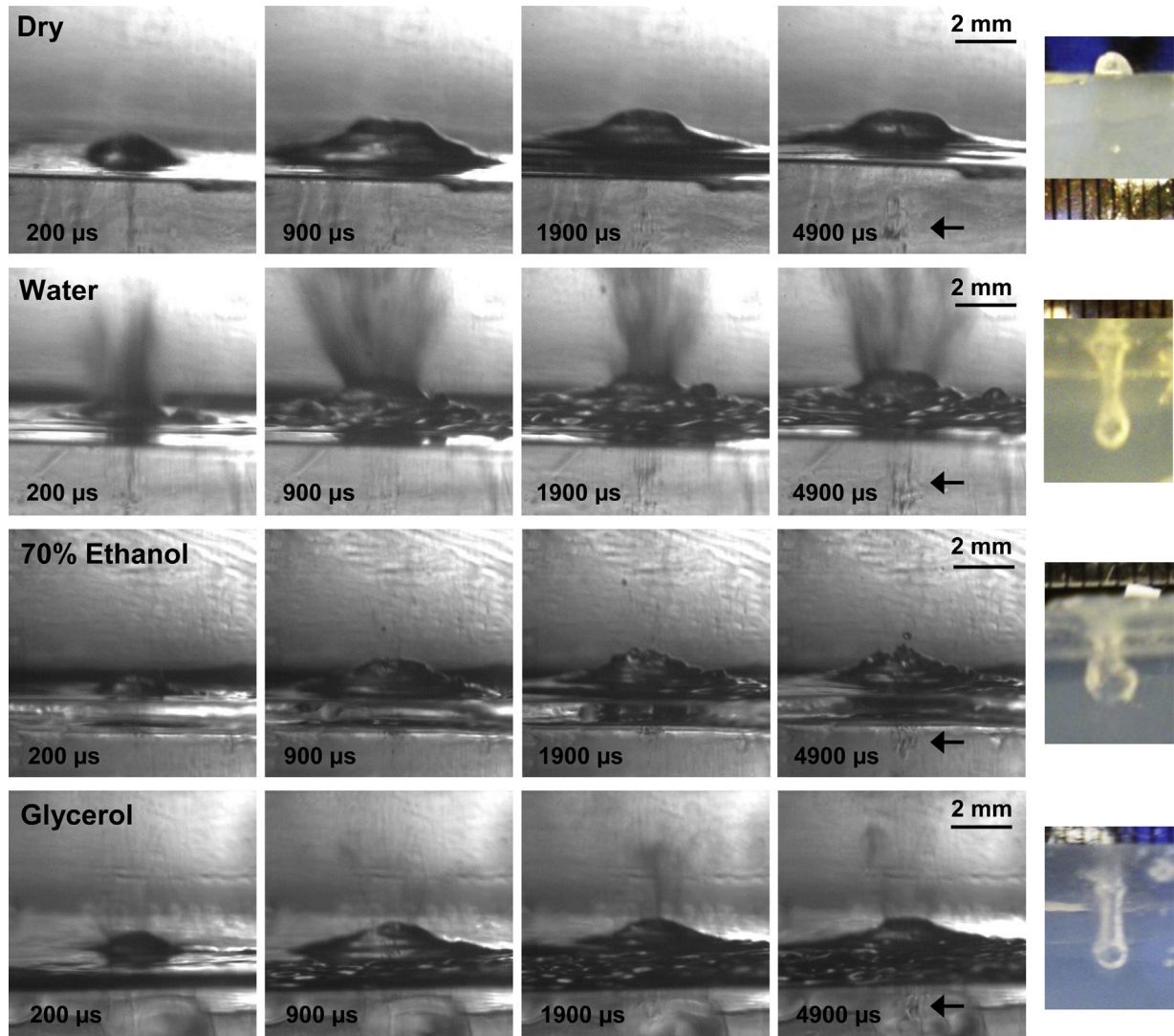


Fig. 7. Selected frames from the high-speed video of tissue-mimicking polyacrylamide gel atomization at the dry, water-wetted, 70% ethanol-wetted, and glycerol-wetted gel surface (rows from top to bottom). In the last column are photographs looking through the gel at the depth of the eroded cavity after sixty 10-ms HIFU pulses repeated at 1 Hz. When the gel surface is dry, frames from the high-speed video reveal that a mound forms in the gel with subsurface cavitation activity (indicated by an *arrow* in fourth frame), but there is no jetting or atomization. The result of sixty 10-ms HIFU pulses in the dry gel is a mound on the gel surface (as illustrated in the top row, right column). For gel samples wetted with water, 70% ethanol or glycerol, the frames from the high-speed videos reveal that the mound still forms with subsurface cavitation activity closer to the gel surface (indicated by *arrows* in the fourth frame) and that jetting or atomization arises from the surface of the mound. The end results of the wetted exposures are cavities in the gel samples as illustrated in the last column. This figure is shown in video format on-line in [Supplementary Video 2](#) (see the online version at <http://dx.doi.org/10.1016/j.ultrasmedbio.2014.12.022>).

in the gel surface. For all of the liquids except olive oil, the surface diameters of the cavities are similar at 2 mm; the surface diameter of olive oil is slightly smaller at 1.5 mm. The depth of the cavities had more variation, perhaps because of slight differences in the mound curvature and the formation of surface instabilities that depend on the interfacial interactions between the wetting liquid and the gel. For water, *n*-propanol, castor oil and glycerol, cavity depths are similar and range be-

tween 4 and 6 mm. The cavities for 1,3-butanediol, 70% ethanol and olive oil are slightly shallower and range between 2.5 and 3 mm in depth.

#### *In vivo liver atomization*

In [Figure 8](#) are selected frames from the high-speed video of atomization of an *in vivo* porcine liver without the capsule at the *in situ* intensity of 16 kW/cm<sup>2</sup>. Atomization begins with the release of liquid jets, followed by

Table 1. Liquid-wetted polyacrylamide gel atomization and erosion descriptors

Liquid	Jet velocity (m/s)*		Emitted drops ( $\mu\text{m}$ )		Mound (mm) <sup>†</sup>		Eroded cavity (mm) <sup>‡</sup>	
	Range	Max	Range	Max	Width	Height	Width	Depth
None, dry	N/A	N/A	N/A	N/A	3.8	0.9	N/A	N/A
Water	5–8	17	20–60	200	3.1	0.7	2	5
1,3-Butanediol	5–8	16	60–200	360	2.6	0.9	2	3
Olive oil	4–7	13	100–200	200	3.5	1.1	1.5	2.5
<i>n</i> -Propanol	6–8	8	20–60	60	3.2	1.1	2	5.5
70% Ethanol	6–8	13	20–60	160	3.1	0.8	2	3
Castor oil	2–4	7	100–400	1,500	2.9	1.2	2	6
Glycerol	4–6	10	20–100	300	3.1	0.9	2	4

\* Ranges for jet velocities and emitted drops are the median jet velocities and droplet diameters, though they range up to the maximum jet velocity or drop diameter.

<sup>†</sup> Mound dimensions were taken at 7.4 ms into the 10-ms pulse.

<sup>‡</sup> Eroded cavity dimensions are to the nearest 0.5 mm, and were measured after sixty 10-ms pulses repeated at 1 Hz. The liquid was added to the gel surface at least 2 min before the exposure began.

the formation of a small tissue or liquid mound that enhances atomization. Droplets of diverse sizes ranging from 1 pixel (20  $\mu\text{m}$ ) to 260  $\mu\text{m}$  are generally released at velocities of 6–10 m/s, though a few jets reach up to 15 m/s. In some cases, near the end of the 10-ms pulse, the number of jets released decreases, perhaps because of the depletion of surface blood. The end result of atomization is erosion from the tissue surface (Fig. 9a). Because of the breathing motion of the pig and the resulting visual maintenance of transducer position, erosion tracks are observed in the tissue surface, rather than the discrete cavities that were observed in *ex vivo* tissues. A section of tissue spanning the erosion tracks was analyzed histologically as illustrated in Figure 9b; blood pooling is observed beneath the tissue surface (*solid arrows*), with evidence of liver cells torn from the surface at the erosion site (*dashed arrows*). There is no evidence of gross thermal injury near or below the targeted region, and there is no evidence of subsurface boiling histotripsy.

In addition to the attempts to atomize the *in vivo* porcine liver without the capsule, another series of exposures were conducted on the intact capsule. Figure 10a illustrates attempted atomization of the dry intact

porcine liver capsule. From these two images taken from the high-speed video, it is apparent that although the surface of the liver becomes convex from the radiation force, no droplets are released and there is no damage to the liver capsule. Then, the liver capsule surface was wetted with saline and atomization was attempted again, as illustrated in Figure 10b. As in the dry capsule exposure, the liver surface becomes convex with the addition of a liquid fountain and significant atomization. Yet the liver capsule is not breached when wetted with saline; no bleeding is observed during the exposure, and the histology reveals no disruption in the layer of two or three cells comprising the liver capsule (Fig. 10c, inset). Tissue fractionation along with blood pooling and even some mild thermal injury extends 2.5 mm beneath the tissue surface in Figure 10c; in other samples, the injury extends up to 4.6 mm beneath the tissue surface. The other wetting liquid that was tested was a surfactant. During the surfactant-wetted exposures, three of the five treatment locations begins to bleed after 3 to 4 min of continuous HIFU pulsing (with the breathing motion of the pig, we expect that this corresponds to fewer than 60 pulses in an isolated location). During the

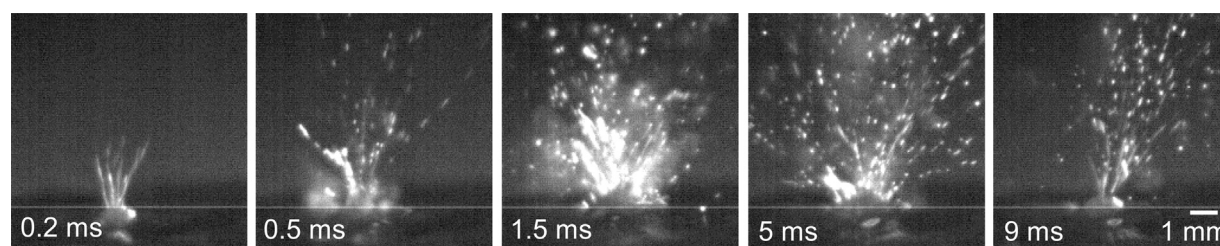


Fig. 8. Select frames from the high-speed video of *in vivo* porcine liver atomization without the capsule. At 0.2 ms, there is already jetting from a small mound in the tissue or in the blood wetting the tissue surface. By 0.5 ms, more jets of various sizes are being emitted from the tissue surface in addition to a fog of very small droplets. As the HIFU pulse continues, more jets are emitted from the tissue surface; however, in this case, near the end of the 10-ms pulse, the number of emitted jets decreases, perhaps because of the depletion of surface blood. This figure is shown in video format on-line in Supplementary Video 3 (see the online version at <http://dx.doi.org/10.1016/j.ultrasmedbio.2014.12.022>).

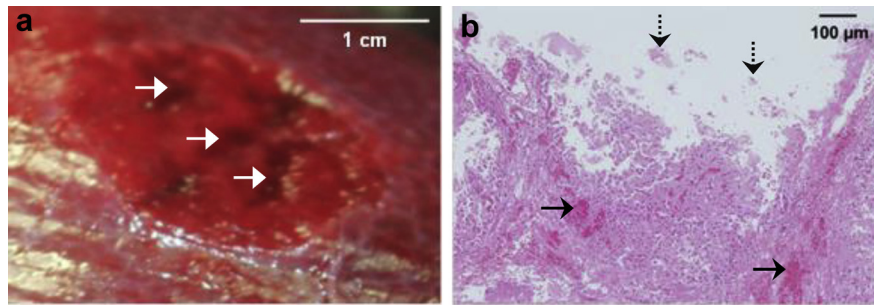


Fig. 9. (a) Photograph of the porcine liver surface without the capsule after the atomization exposure. Three tracks are visible in the surface (indicated by *white arrows*), rather than discrete cavities, because of the breathing motion of the pig and other experimental arrangement constraints. (b) Hematoxylin and eosin-stained histology image spanning one of the tracks in the liver surface. Blood pooling (indicated by *solid black arrows*) is observed beneath the cavity in the tissue surface, and the tissue appears torn away (some fragments indicated by *dashed black arrows*) from the bulk liver. No cellular desiccation or evidence of thermal injury is visible in the histology section.

exposure, a significant amount of bruising is observed beneath the capsule surface before the breach occurs. This is similar to what was observed when the liver capsule was wetted with saline, though the capsule never was breached. In [Figure 11](#) are frames from a high-speed video taken during the surfactant-wetted HIFU exposure of the intact liver capsule. As in the other *ex vivo* and *in vivo* exposures, atomization begins with the initial jetting of fine particles followed by the formation of a mound. As the 10-ms pulse continues, a surfactant fountain and surface waves form on the liver capsule and substantially increase atomization. The end result of the surfactant-wetted exposure is a small breach in the liver capsule as evidenced by bleeding during the exposure. The jet velocities in this video are approximately 10

m/s, with ejected droplets ranging from 1 pixel (20  $\mu\text{m}$ ) to 720  $\mu\text{m}$  in diameter.

#### Atomization and recirculation

[Figure 12](#) illustrates the results of repeated atomization in a confined volume. Only cellular debris with a few dying cells are present throughout the histology sample, with no whole cells or nuclei. The total HIFU exposure time was approximately 3 min; however, motion of the tissue sample out of the transducer focus leads to the supposition that fewer pulses are needed to fully fractionate bulk tissue. These results concur with what is observed after boiling histotripsy exposures and confirm our hypothesis that recirculation of the fountain projectiles is necessary for complete tissue homogenization.

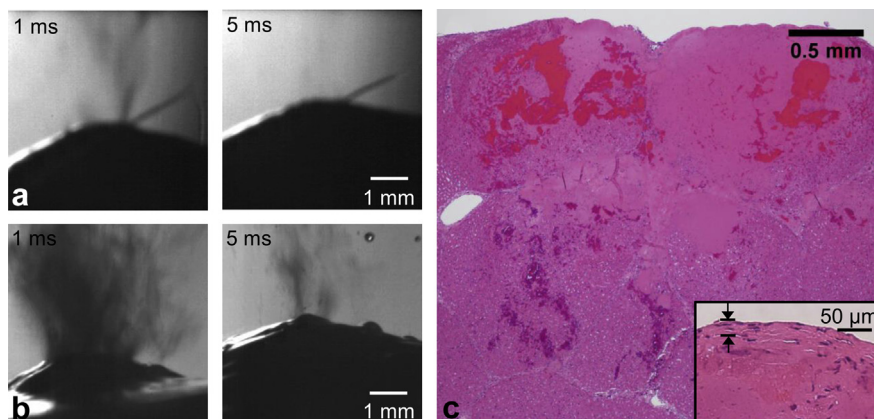


Fig. 10. (a) High-speed video frames of *in vivo* dry liver capsule atomization. A fog of droplets is released initially, perhaps because of the natural wetness of the liver before, atomization ceases. The line just to the right of the tissue mound is a stray hair as opposed to an atomized jet. (b) High-speed video frames of saline-wetted liver capsule atomization. In this case, atomization begins immediately and continues throughout the 10-ms pulse. Yet the liver capsule does not breach as illustrated in the hematoxylin and eosin-stained histology slide in (c). (c) The large image reveals that for this example the injury extends approximately 2.5 mm beneath the tissue surface. The inset reveals that the layer of two or three cells constituting the liver capsule remains intact (thickness of the intact capsule indicated by *arrows*) with almost complete mechanical fractionation of the tissue immediately below the liver capsule cells. (a) and (b) are shown in video format online in [Supplementary Video 4](#) (see the online version at <http://dx.doi.org/10.1016/j.ultrasmedbio.2014.12.022>).

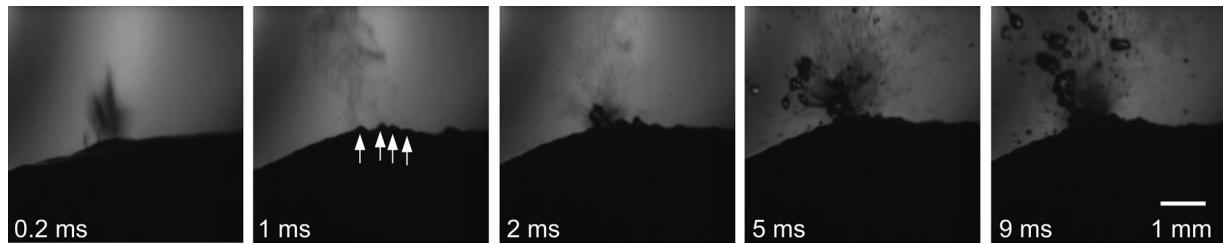


Fig. 11. High-speed video frames of surfactant-wetted *in vivo* liver capsule atomization. In the first frame at 0.2 ms, the mound in the tissue surface is forming and the initial jets are being released from the capsule surface. By the second frame taken at 1 ms, a fog of droplets continues to be released, and surface waves (crests indicated by white arrows) are visible on or within the liver capsule. These waves continue to form on the capsule, and a fountain has developed by 2 ms. The fountain and surface waves enhance atomization and cause a breach to form in the liver capsule, as evidenced by bleeding during the atomization exposure. This figure is shown in video format on-line in [Supplementary Video 5](#) (see the online version at <http://dx.doi.org/10.1016/j.ultrasmedbio.2014.12.022>).

## DISCUSSION

Evidence from these studies supports both surface instabilities and bubble activity as contributors to tissue atomization. In the first study, overpressure was used to illustrate that bubbles are important to tissue fractionation by atomization; as the static pressure of the system increased, the degree of tissue fractionation decreased. It was difficult to discern whether these bubbles arose from acoustic cavitation or heat deposition and boiling. That there was no apparent change in the appearance of atomization in the high-speed videos at the predicted boiling time for each overpressure level would suggest that boiling, if it occurred, played only a minor role in tissue atomization. However, overpressure also caused thermal denaturation rather than ejection of the fractionated tissue. At atmospheric pressure, the results suggest that bubble activity beneath the surface, along with surface instabilities and spallation, caused liquefaction and atomization of the initially intact tissue. When the static

pressure is increased, bubble activity is reduced (Bailey *et al.* 2001), slowing the rates of tissue liquefaction and atomization, as evidenced by the frames from the high-speed videos in [Figure 3](#) and the histology images in [Figure 5](#). Thermal denaturation occurs when the reduction in bubble activity and atomization causes the tissue to spend more time at the transducer focus.

A change in the atomized droplets is also observed in the overpressure studies; when the static pressure is increased to even 1.4 MPa, the droplets are uniformly small in diameter and emitted at less than half the velocity observed at atmospheric pressure. As the appearance of atomization did not change throughout the high-speed video (100  $\mu$ s resolution), it is unlikely that thermal denaturation explains the change in the emitted droplets. It is also unlikely that capillary waves describe the mechanism of droplet release because the droplets are only emitted from the peak of the liver mound rather than distributed across the entire mound surface. Rather, we hypothesize that spallation is one of the atomization mechanisms at atmospheric pressure and becomes the dominant mechanism of tissue fragment release under hyperbaric conditions.

Additionally, in the overpressure experiments, a cavity is generated approximately 3 mm beneath the tissue surface for static pressure levels between 1.4 and 3.4 MPa, yet is not observed consistently at 6.9 MPa. One explanation for the cavity in tissue is boiling; at 3.4 MPa, the boiling temperature of water is 242°C (EngineeringToolbox.com 2013). According to the weak shock theory, with an *in situ* shock amplitude of 70 MPa, boiling is predicted in approximately 8 ms (Canney *et al.* 2010). When the static pressure is 6.9 MPa, the boiling temperature of water increases to 285°C (EngineeringToolbox.com 2013), in which case boiling is predicted in approximately 10 ms. As individual HIFU pulses are only 10 ms in duration, the cavity could be a result of boiling initiation within each HIFU pulse. However, it is also possible the cavity forms

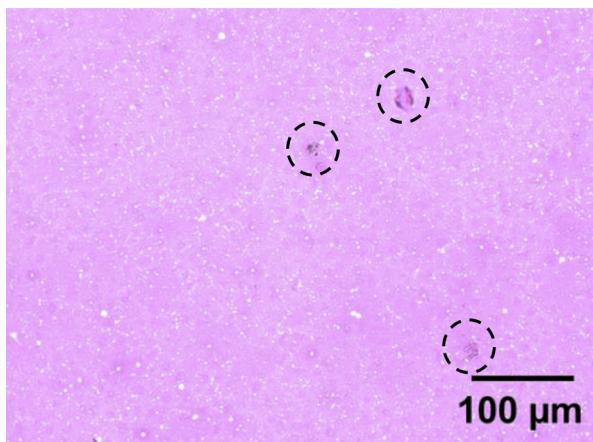


Fig. 12. Hematoxylin and eosin-stained histology image revealing cellular debris and bubbles after recirculation of the fountain projectiles. A few damaged cells remain in the sample as indicated by the *dashed circles* in the figure.

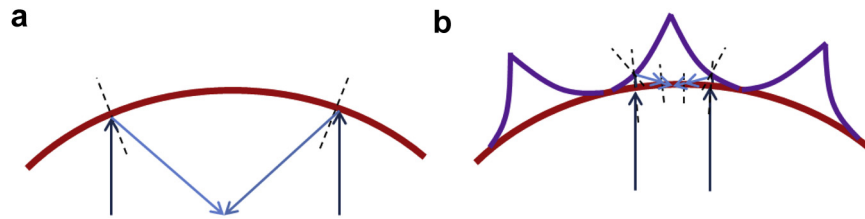


Fig. 13. Magnified schematic of the hypothesis proposed to explain how wetting the surface of an elastic tissue or tissue-mimicking gel enhances atomization to erode the surface. (a) Diagram approximating the curvature of the dry tissue-mimicking gel surface and the interaction of the ultrasound wave with the pressure-release interface. These approximations illustrate the reflected wave refocusing well beneath the tissue surface, where we would expect intense cavitation to occur and fractionate the tissue or gel. However, when the gel or elastic tissue surface is wetted as illustrated in (b), the liquid will form surface capillary-type waves and/or fountains. Once the surface waves form, the geometry of the surface changes, so the ultrasound wave refocuses at or near the gel or tissue surface. Intense cavitation at the viscoelastic surface from this refocusing could cause atomization and surface erosion to be successful.

from acoustic cavitation; when the mound is at its maximum height (approximately 2.5 mm), the transducer focus is located in the same position as the cavity (with its center approximately 2.5 mm beneath the tissue surface). Therefore, with these parameters it is difficult to discern whether acoustic cavitation bubbles or boiling bubbles form the tissue cavity under hyperbaric conditions.

The results from the tissue wetness and *in vivo* studies suggest that surface wetting can enhance atomization. Analysis of the high-speed videos and erosion volumes indicates that atomization occurs similarly (if not more efficiently) when the capsule is removed in the *in vivo* porcine liver than in *ex vivo* bovine liver perhaps because of the continuous surface wetting from the blood. Additionally, in the surface wetness studies, it was found that wetting the surface of a tissue-mimicking polyacrylamide gel caused atomization and erosion, whereas the dry gel surface did not atomize or erode. Even wetting the gel surface with liquids that do not atomize on their own and are rather robust to cavitation, such as glycerol and castor oil (Simon et al. 2012), causes atomization and erosion when the liquids are spread in a thin layer across the gel surface. Furthermore, atomization breaches the intact *in vivo* porcine liver capsule when wetted with a low-surface-tension liquid or a surfactant. One possible explanation of why surface wetting enhances atomization is that when the viscoelastic surface is dry, the mound curvature refocuses the reflected and inverted wave deep within the gel or liver as illustrated in Figure 13a; however, when the elastic surface is wetted, fountains or capillary waves form in the liquid on the gel or liver surface, causing the inverted and reflected wave to refocus at or near the viscoelastic surface, as sketched in Figure 13b. Intense acoustic cavitation at the focus of the inverted and reflected wave causes fractionation below the gel or liver surface (when dry) or erosion of the gel or liver surface (when wetted). Such acoustic cavitation is visible in the frames from the high-speed videos of atomization in the transparent, tissue-mimicking, polyacrylamide gel

in Figure 7. Although the properties of the wetting liquid were not important in the gel, only surfactant wetting of the *in vivo* liver capsule caused a breach to form in the capsule. It is possible that the surface instability wavelength is too long in saline, causing the inverted and reflected wave to refocus too deep within the tissue to cause the breach. This is evidenced by the tissue injury extending up to 4.6 mm beneath the tissue surface. The surfactant has lower surface tension and, therefore, a shorter instability wavelength, potentially causing the inverted and reflected wave to refocus more closely to the capsular surface and forming the breach.

These studies provide some basic insights into the mechanisms of tissue atomization, which adds some practical information for the boiling histotripsy clinical application. For example, the threshold for atomization or fractionation is highly dependent on the tissue type, and there may be techniques to control the atomization threshold through surface wetting or use of contrast agents to enhance cavitation. Another example of how these results relate to the design and practice of boiling histotripsy is in the choice of ultrasound frequency; cavitation can be reduced with frequency, but the gradient of surface deformations from the tighter focus may enhance surface effects. This work also indicates that repeated HIFU pulsing is needed to fully break up cells into a tissue homogenate, which is an important consideration for future cancer treatment by boiling histotripsy. Although these results were primarily experimental in nature, they enhance our understanding of the atomization mechanism of boiling histotripsy, which is important as boiling histotripsy transitions into a clinical therapy.

**Acknowledgments**—The authors thank our collaborators at the Center for Industrial and Medical Ultrasound. In particular, we thank Dr. Ziyue Liu at Indiana University for performing the statistical analysis on the large amounts of data collected in the bulk tissue wetness studies. We also thank Ameen Tabatabai for his help in the bulk wetness studies, Frank (Rusty) Starr III for his help in the *in vivo* studies, Dr. Wayne Kreider for his helpful discussions in bubble dynamics and Brian MacConaghy for designing, building and testing the overpressure chamber.

In addition, we thank Viaspan for donating 2 L of solution for evaluation of *ex vivo* tissue preservation. We also thank our funding sources, including the National Space Biomedical Research Institute in consortium agreement with the National Aeronautics and Space Administration NCC 9-58, the National Institutes of Health (DK043881 and EB007643) and the Russian Foundation for Basic Research (13-02-00183 and 14-02-00426).

## SUPPLEMENTARY DATA

Supplementary data related to this article can be found at <http://dx.doi.org/10.1016/j.ultrasmedbio.2014.12.022>

## REFERENCES

- Albaugh E, Amador B, Molin J, Poloney D, Savage A. Medical microbiology/soap. Terra-Haute, IN: Rose-Hulman Institute of Technology; 2008.
- Bailey MR, Couret LN, Sapozhnikov OA, Khokhlova VA, ter Haar G, Vaezy S, Shi X, Martin R, Crum LA. Use of overpressure to assess the role of bubbles in focused ultrasound lesion shape in vitro. *Ultrasound Med Biol* 2001;27:695–708.
- Bessonova OV, Khokhlova VA, Canney MS, Bailey MR, Crum LA. A derating method for therapeutic applications of high intensity focused ultrasound. *Acoust Phys* 2010;56:354–363.
- Boguslavskii YY, Eknadiosyants OK. Physical mechanism of the acoustic atomization of a liquid. *Sov Phys Acoust* 1969;15:14–21.
- Boutilier RG. Mechanisms of cell survival in hypoxia and hypothermia. *J Exp Biol* 2001;204:3171–3181.
- Brockbank KGM, Taylor MJ. Tissue preservation. In: Baust JG, Baust JM, (eds). *Advances in biopreservation*. Ebook. Boca Raton, FL: CRC Press; 2006. p. 157–196.
- Bronskaya LM, Vigderman VS, Sokol'skaya AV, El'piner IE. Influence of the static pressure on ultrasonic chemical and biological effects. *Sov Phys Acoust* 1968;13:374–375.
- Canney MS, Bailey MR, Crum LA, Khokhlova VA, Sapozhnikov OA. Acoustic characterization of high intensity focused ultrasound fields: A combined measurement and modeling approach. *J Acoust Soc Am* 2008;124:2406–2420.
- Canney MS, Khokhlova VA, Bessonova OV, Bailey MR, Crum LA. Shock-induced heating and millisecond boiling in gels and tissue due to high intensity focused ultrasound. *Ultrasound Med Biol* 2010;36:250–267.
- EngineeringToolbox.com. The engineering toolbox. Available at: <http://www.engineeringtoolbox.com>; 2013.
- Hill CR. Ultrasonic exposure thresholds for changes in cells and tissues. *J Acoust Soc Am* 1971;51:667–672.
- Kaboyashi T, Sumimoto R, Shimada H, Kamada N, Nakagawara G. Effect of sugars in the preservation liver storage in rats. *Cryobiology* 1991;28:428–435.
- Khokhlova T, Wang YN, Simon J, Cunitz B, Starr F, Paun M, Crum L, Bailey M, Khokhlova V. Ultrasound-guided tissue fractionation by high intensity focused ultrasound in an *in vivo* porcine liver model. *Proc Natl Acad Sci USA* 2014;111:7974–7979.
- Khokhlova TD, Canney MS, Khokhlova VA, Sapozhnikov OA, Crum LA, Bailey MR. Controlled tissue emulsification produced by high intensity focused ultrasound shock waves and millisecond boiling. *J Acoust Soc Am* 2011;130:3498–3510.
- Khokhlova VA, Bailey MR, Reed JA, Cunitz BW, Kaczkowski PJ, Crum LA. Effects of non-linear propagation, cavitation, and boiling in lesion formation by high intensity focused ultrasound in a gel phantom. *J Acoust Soc Am* 2006;119:1834–1848.
- Lafon C, Zderic V, Noble ML, Yuen JC, Kaczkowski PJ, Sapozhnikov OA, Chavrier F, Crum LA, Vaezy S. Gel phantom for use in high-intensity focused ultrasound dosimetry. *Ultrasound Med Biol* 2005;31:1383–1389.
- Lam FT, Mavor AID, Potts DJ, Giles GR. Improved 72-h renal preservation with phosphate-buffered sucrose. *Transplantation* 1989;47:767–771.
- Little JR. Determination of water and electrolytes in tissue slices. *Anal Biochem* 1964;7:87–95.
- Rozenberg LD, (ed). *Physical principles of ultrasonic technology*, 2. New York: Plenum Press; 1973.
- Sapozhnikov OA, Khokhlova VA, Bailey MR, Williams JC, McAteer JA, Cleveland RO, Crum LA. Effect of overpressure and pulse repetition frequency on cavitation in shock wave lithotripsy. *J Acoust Soc Am* 2002;112:1183–1195.
- Simon JC, Sapozhnikov OA, Khokhlova VA, Wang YN, Crum LA, Bailey MR. Ultrasonic atomization of tissue and its role in tissue fractionation by high intensity focused ultrasound. *Phys Med Biol* 2012;57:8061–8078.
- Simon JC. The thresholds and mechanisms of tissue injury by focused ultrasound. Doctoral dissertation. Seattle: University of Washington, ProQuest/UMI; 2013.
- Southard JH. The right solution for organ preservation. *Business Briefing Global Surg* 2004;16:79–84.
- Sunderman FW, Williams P. Diminution in chloride measurement after drying blood and tissues. *J Biol Chem* 1931;92:99–107.
- Vlaisavljevich E, Kim Y, Owens G, Roberts W, Cain C, Xu Z. Effects of tissue mechanical properties on susceptibility to histotripsy-induced tissue damage. *Phys Med Biol* 2014;59:253–270.
- Wang YN, Khokhlova T, Bailey M, Hwang JH, Khokhlova V. Histologic and biochemical analysis of mechanical and thermal bioeffects in boiling histotripsy lesions induced by high intensity focused ultrasound. *Ultrasound Med Biol* 2013;39:424–438.